Journal of Marine Science and Application (2024) 23: 113-126
https://doi.org/10.1007/s11804-024-00385-7

RESEARCH ARTICLE

Analysis of Wave-Induced Forces on a Floating Rectangular Box with Analytical and Numerical Approaches

Sarat Chandra Mohapatra[1], Iuri Baldaconi da Silva Bispo[1], Yuchan Guo[1] and C. Guedes Soares[1]

Received: 15 January 2023 / Accepted: 24 May 2023

Abstract
A three-dimensional mathematical hydrodynamic model associated with surface wave radiation by a floating rectangular box-type structure due to heave, sway, and roll motions in finite water depth is investigated based on small amplitude water wave theory and linear structural response. The analytical expressions for the radiation potentials, wave forces, and hydrodynamic coefficients are presented based on matched eigenfunction expansion method (MEFEM). The correctness of the analytical results of wave forces is compared with the construction of a numerical model using the open-source boundary element method code NEMOH. In addition, the present result is compared with the existing published experimental results available in the literature. The effects of the different design parameters on the floating box-type rectangular structure are studied by analyzing the vertical wave force, horizontal wave force, torque, added mass, and damping coefficients due to the heave, sway, and roll motions, and the comparison analysis between the forces is also analyzed in detail. Further, the effect of reflection and transmission coefficients by varying the structural width and drafts are analyzed.

Keywords Mathematical model; MEFEM; Box-type structure; BEM code NEMOH; Wave forces

1 Introduction

In the last half-century, floating structures of various configurations are being studied due to their significant importance in the field of ocean and coastal engineering. Different types of rigid floating structures are constructed near the coastal region, which is aimed at ocean space utilization for various human activities, marine activities, and coastal zone management such as sea walls, jetties, piers, breakwaters, floating platforms for oil exploration and ship navigation, wave energy devices, etc. One of the most interesting floating breakwater types is the box type which is effective in moderate conditions (McCartney, 1985; Bhattacharjee and Guedes Soares, 2011; Gadelho et al., 2018; Islam et al., 2019). When the floating structures are constructed in a coastal region/nearshore, it is important to develop a three-dimensional body for application in engineering practice. Therefore, the three-dimensional mathematical modeling of hydrodynamic analysis based on the analytical study of floating structures and comparative analysis is of recent interest to coastal researchers and engineers to design an effective floating breakwater.

The study of the radiation problem on floating rectangular structures can provide fundamental information on the hydrodynamic characteristics of wave forces, added mass, and radiation damping of the floating structure. Under the excitation of waves, a rigid floating body will exhibit six degrees of freedom (DOF), namely three translations and three rotational motions. Translation motions are referred to as heave, sway, and surge, and rotational motions are referred to as pitch, yaw, and roll. Physically, vertical (heave), horizontal (sway), rotational (roll) motions, reflection coefficients, and transmission coefficients are of primary importance to analyze the hydrodynamic interaction of ocean waves with floating rectangular structures in three-dimension wave incidence.

Article Highlights

- A mathematical hydrodynamic model of surface wave radiation by a floating rectangular box-type structure is developed in three dimensions.
- Using the MEFEM, the analytical solutions for hydrodynamic coefficients are obtained.
- The analytical results are compared with a numerical open-source boundary element method code NEMOH and existing published experimental datasets.
- The performance of the model is studied by analyzing the hydrodynamic coefficients as well as the reflection and transmission coefficients.

✉ Sarat Chandra Mohapatra
sarat.mohapatra@centec.tecnico.ulisboa.pt

[1] Center for Marine Technology and Ocean Engineering (CENTEC), Instituto Superior Técnico, Universidade de Lisboa, Lisboa 1049-001, Portugal

In this class of problems, the mathematical difficulty is the non-homogeneous boundary condition at the structure surface which can be handled with the help of the partial differential solution method. Therefore, the analytical solutions shown in the literature have generally been obtained using boundary matching techniques to solve the problem under linearized water wave theory for predicting the hydrodynamic characteristics of floating structures to set the benchmark. The MEFEM has been used in the study of the hydrodynamic interaction of floating rectangular structures due to its considerable accuracy and less use of computer memory and as well as processing time in three dimensions (Mohapatra and Guedes Soares, 2021; 2022). Further, the series solutions using the eigenfunction expansion attend the convergence for the wave forces and hydrodynamic coefficients of a floating structure in two-dimensions and oblique wave cases (Bhattacharjee and Guedes Soares, 2011; Guo et al., 2018; Islam et al., 2019).

Previously, many papers have been involved in the hydrodynamic analysis of floating rectangular structures to obtain hydrodynamic coefficients, wave forces, reflection coefficients, and transmission coefficients based on analytical/semi-analytical methods. Drimer et al. (1992) developed a simplified model associated with a fully linearized hydrodynamic problem to study the performance of a two-dimensional box-type floating breakwater in finite water depth. Lee (1995) presented an analytical solution for the heave radiation of a floating rectangular structure to analyze the hydrodynamic effects of the submergence and width of the structure. Zheng et al. (2004) used the MEFEM to analyze the radiation and diffraction of linear water waves by a rectangular buoy in the water of finite depth in two dimensions. Zheng et al. (2006) used an eigenfunction expansion method to investigate the oblique wave radiation by a floating rectangular structure in finite water depth over a flat seabed. Cho (2016) analyzed the effects of porosity and protruding depth of the vertical side plates on the transmission coefficients and motion response of a floating rectangular breakwater based on matched eigenfunction expansion method. Elchahal et al. (2009) developed a diffraction-radiation boundary value problem (BVP) to study the hydrodynamic performance of the moored floating rectangular breakwater by considering the effect of the side wall, structural parameters, mooring stiffness, angle of incidence on the transmission coefficients and dynamic motion of the floating breakwater. Recently, Guo et al. (2018) analyzed the oblique wave diffraction by a long rectangular rigid floating structure over flat bottom based on linearized water wave theory. Gadelho et al. (2018) studied the CFD analysis of fixed floating box-type structures and compared it with linearized Boussinesq analytical solution and experimental data by analyzing the wave elevations before and after the floating box-type structure and wave forces on the box over the flat bottom. Islam et al. (2019) studied the comparison of CFD, linearized analytical of the oblique wave, and experimental data results of a heaving box-type floating structure. Bhattacharjee and Guedes Soares (2011) studied the effect of the oblique angle and bottom on wave diffraction by a floating rectangular structure over stepped bottom with a rigid wall. Islam et al. (2019) studied the wave radiation by a floating box-type structure over the flat bottom in two dimensions. All the investigations discussed above are assumed to be in two-dimensional and oblique wave incident wave analysis.

From the above literature, it is confirmed that there is no analysis of the wave-induced forces based on the three-dimensional mathematical model solution and comparison with BEM code NEMOH to date to the authors' knowledge.

Therefore, in the present study, the main and new contributions compared with Guo et al. (2018) and Islam et al. (2019) are the 1) mathematical formulation associated with wave radiation by a three-dimensional floating rectangular box and the analytical expression for the radiational potentials (by adding finite structural width), 2) analytical expressions for the hydrodynamic coefficients, added mass, damping coefficients, and wave forces for the heave, sway and roll motions, 3) comparison between the present and the independent numerical BEM code based NEMOH simulations, 4) analysis of the wave forces and hydrodynamic coefficients on heave, sway, and roll motions for modes of oscillations, structural width, and comparison among them from the analytical solutions. Further, the results for the reflection and transmission coefficients for different values of structural width and drafts are presented and also analyzed. Finally, some significant concluding remarks from the present analysis are discussed.

2 Mathematical formulation of floating rectangular box model in 3D

The mathematical model of the BVP is considered in a three-dimensional Cartesian coordinate system (x, y, z) with $x - z$ being in the horizontal plane that coincides with undisturbed water surface and the y-axis being in the vertical downward positive direction. The wave radiation is due to the heave, sway, and roll motions of a rectangular box-type structure floating on the free surface of length $2l$, width b, and draft d. The origin o is assumed to be the middle point of the box (as in Figure 1). Hence, the whole fluid domain is divided into three regions as defined by: $(l<x<\infty,\ 0<y<h,\ 0\leqslant z\leqslant b)$, $(-l<x<l,\ d<y<h,\ 0\leqslant z\leqslant b)$ and $(-l<x<-\infty,\ 0<y<h,\ 0\leqslant z\leqslant b)$ are referred to as R_1, R_2, and R_3, respectively.

The water is assumed to be inviscid, and incompressible and the flow is irrotational and simple harmonic in time with angular frequency ω. Thus, there exists a velocity potential $\Phi(x, y, z, t) = \mathrm{Re}\ \{\phi(x, y, z)\exp(-\mathrm{i}\omega t)\}$, where

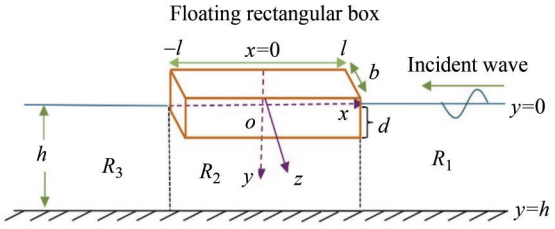

Figure 1 Nomenclature of the problem

Re denotes the real part of the complex expression and $\phi(x,y,z)$ denotes the spatial velocity potential which satisfies the three-dimensional Laplace equation as given by

$$\nabla^2_{xyz}\phi = 0 \text{ in the fluid domain} \tag{1}$$

where $\nabla^2_{xyz} = \partial^2/\partial x^2 + \partial^2/\partial y^2 + \partial^2/\partial z^2$.

The velocity potential $\phi(x,y,z)$ is decomposed into the incident wave potential, the diffracted potential (due to the stationarity of the structure), and the radiation potential (due to the heave, sway, and roll motions of the floating structure) are denoted by ϕ_I, ϕ_D, and ϕ_R respectively. So the total potential $\phi(x,y,z)$ can be expressed as

$$\phi = \phi_I + \phi_D + \sum_{S=1}^{3}\phi_R^{(S)} \tag{2}$$

where $S = 1, 2$ and 3 stand for heave, sway, and roll motions, respectively.

The incident wave potential of linear waves propagating to the negative x- and z-direction is given by

$$\phi_I(x,y,z) = \sum_{m=1}^{\infty}\frac{igI_{m0}}{\omega}\frac{\cosh k_0(h-y)}{\cosh k_0 h}\cos\gamma_m z e^{-ip_{m0}x} \tag{3}$$

where $\gamma_m = m\pi/b$ for $m = 1, 2, 3, ...$, are referred to as primary, secondary, tertiary, and other higher modes, respectively with $p_{m0}^2 = (k_0^2 - (\gamma_m)^2) > 0$ to ensure that progressive wave solution exists (as in Mohapatra and Guedes Soares, 2019), g signifies the gravitational constant, I_{m0} is the incident wave amplitude with the dimension of unit length, and wavenumber k_0 associated with the incident wave which satisfies the gravity wave dispersion relation as $\omega^2 = gk_0\tanh(k_0 h)$.

Small motions of the floating three-dimensional rectangular box shown in Figure 1 are assumed. If the amplitude of the motion of the rectangular box is assumed as $I_R^{(S)}$, the radiation potential $\phi_R^{(S)}(x,y,z)$ in three-dimensions

$$\phi_R^{(S)}(x,y,z) = \mathrm{Re}\left[-i\omega I_R^{(S)}\varphi_R^{(S)}(x,y,z)\right] \tag{4}$$

where $\varphi_R^{(S)}(x,y,z)$ is the spatial velocity potential satisfying the three-dimensional Laplace equation as

$$\frac{\partial^2\varphi_R^{(S)}}{\partial x^2} + \frac{\partial^2\varphi_R^{(S)}}{\partial y^2} + \frac{\partial^2\varphi_R^{(S)}}{\partial z^2} = 0 \tag{5}$$

Combining the kinematic and dynamic boundary conditions, the linearized boundary condition at the mean free surface is obtained as

$$\frac{\partial\varphi_R^{(S)}}{\partial y} + K\varphi_R^{(S)} = 0 \text{ on } y = 0,\ 0 \leqslant z \leqslant b \text{ for } R_1 \text{ and } R_3 \tag{6}$$

where $K = \omega^2/g$. The no-flow conditions at the rigid bottom boundary are given by

$$\frac{\partial\varphi_R^{(S)}}{\partial y} = 0 \text{ on } y = h \text{ for } R_1, R_2 \text{ and } R_3,\ 0 \leqslant z \leqslant b \tag{7}$$

$$\frac{\partial\varphi_R^{(S)}}{\partial x} = 0 \text{ on } x \in (-l, l),\ y = d,\ 0 \leqslant z \leqslant b \tag{8}$$

The non-homogeneous boundary condition due to the heave, sway, and roll motions of the floating structure is given by

$$\frac{\partial\varphi_R^{(S)}}{\partial y} = \delta_{1,S} - (x - x_0)\delta_{3,S} \text{ on } -l \leqslant x \leqslant l, y = d, 0 \leqslant z \leqslant b \tag{9}$$

Further, the conditions on the rigid structural boundary are described as

$$\frac{\partial\varphi_R^{(S)}}{\partial x} = \delta_{2,S} + (y - y_0)\delta_{3,S}, \text{ at } x = \pm l, 0 < y < d, 0 \leqslant z \leqslant b \tag{10}$$

where (x_0, y_0) is the centre of rotation for roll motion and δ is Kronecker delta function as defined by

$$\delta_{j,S} = \begin{cases} 0 & \text{for } j \neq S \\ 1 & \text{for } j = S \end{cases} \tag{11}$$

Since the structure is not moving, the no-flow condition at $z = 0, b$ yield

$$\frac{\partial\varphi_R^{(S)}}{\partial z} = 0 \text{ at } z = 0, b,\ 0 < y < d \tag{12}$$

Finally, the radiation condition is assumed to take the form

$$\lim_{G\to\mp\infty}\left[\frac{\partial\varphi_R^{(S)}}{\partial G} \pm ip\varphi_R^{(S)}\right] = 0 \text{ for } G = x, z \tag{13}$$

The next Section will obtain the analytical expressions for radiated potentials in each region and their solutions by satisfying the governing equations along with the relevant boundary conditions.

3 Analytical solution based on the MEFEM

The analytical solutions for the radiation potentials are obtained using the MEFEM of the discussed BVP. The radiation potentials in R_1, R_2 and R_3 are denoted by $\varphi_{R1}^{(S)}, \varphi_{R2}^{(S)}$ and $\varphi_{R3}^{(S)}$, respectively. The expressions for the radiation potentials in each region are obtained by applying the method of separation of variables and the unknown coefficients associated with the radiation potentials are then determined by invoking the continuity condition of velocity and pressure at the structural boundary $x = \pm l$ and $0 \leqslant z \leqslant b$.

3.1 Analytical expressions for the radiation potentials in each region

Using the Fourier expansion formulae in three regions R_1, R_2 and R_3, the radiation potentials $\varphi_{R1}^{(S)}(x,y,z)$, $\varphi_{R2}^{(S)}(x,y,z)$ and $\varphi_{R3}^{(S)}(x,y,z)$ respectively satisfying the three-dimensional Laplace Equation (5) along with the relevant boundary conditions (7)–(13) are expanded as

$$\varphi_{R1}^{(S)} = \sum_{m=1}^{\infty}\left\{A_{1m0}^{(S)}\mathrm{e}^{\mathrm{i}p_{m0}(x-l)}u_{m0}(y,z) + \sum_{n=1}^{\infty}A_{1mn}^{(S)}\mathrm{e}^{p_{mn}(x-l)}u_{mn}(y,z)\right\} \tag{14}$$

$$\varphi_{R2}^{(S)} = \sum_{m=1}^{\infty}\left\{\frac{-\cosh\alpha_{m0}(h-y)}{\alpha_{m0}\sinh\alpha_{m0}(h-d)}\cos\gamma_m z\,\{\delta_{1,S} - (x-x_0)\delta_{3,S}\} + \sum_{n=0}^{\infty}\left[A_{2mn}^{(S)}\mathrm{e}^{-\alpha_{mn}(x-l)} + B_{2mn}^{(S)}\mathrm{e}^{\alpha_{mn}(x+l)}\right]v_{mn}(y,z)\right\} \tag{15}$$

$$\varphi_{R3}^{(S)} = \sum_{m=1}^{\infty}\left\{A_{3m0}^{(S)}\mathrm{e}^{-\mathrm{i}p_{m0}(x+l)}u_{m0}(y,z) + \sum_{n=1}^{\infty}A_{3mn}^{(S)}\mathrm{e}^{p_{mn}(x+l)}u_{mn}(y,z)\right\} \tag{16}$$

where, the first part in Equation (15) is the particular solution of the radiation potential $\varphi_{R2}^{(S)}$, $p_{mn}^2 = k_n^2 - (\gamma_m)^2$ and $\alpha_{mn}^2 = \beta_n^2 - (\gamma_m)^2$ with $\alpha_{m0}^2 = \beta_0^2 - (\gamma_m)^2 > 0$ and the eigenvalues k_0 is same as defined in Equation (3) and $k_n = \mathrm{i}k_n$, β_ns are satisfy the following dispersion relations

$$\omega^2 = -gk_n\tan(k_n h) \tag{17}$$

$$\beta_n = \frac{n\pi}{(h-d)}\ \text{for}\ n = 0, 1, 2, ... \tag{18}$$

Further, the eigenfunctions $u_{mn}(y,z)$ and $v_{mn}(y,z)$ associated with Equations (14)–(16) are given by

$$\begin{cases} u_{m0}(y,z) = \dfrac{\cosh k_0(h-y)}{\cosh k_0 h}\cos\gamma_m z \\ u_{mn}(y,z) = \dfrac{\cos k_n(h-y)}{\cos k_n h}\cos\gamma_m z \end{cases} \tag{19}$$

$$v_{mn}(y,z) = \cos\beta_n(h-y)\cos\gamma_m z \tag{20}$$

are orthogonal concerning their intervals as defined by

$$\left\langle u_{mn}, u_{jl}\right\rangle = \int_0^b\int_0^h u_{mn}(y,z)\,u_{jl}(y,z)\,\mathrm{d}y\mathrm{d}z = \frac{b}{2}\delta_{mj}\delta_{nl}U_{\mathrm{n}} \tag{21}$$

$$\left\langle v_{mn}, v_{jl}\right\rangle = \int_0^b\int_d^h v_{mn}(y,z)\,v_{jl}(y,z)\,\mathrm{d}y\mathrm{d}z = \frac{b}{2}\delta_{mj}\delta_{nl}V_{\mathrm{n}} \tag{22}$$

where

$$U_n = \begin{cases} \dfrac{1}{2\cosh^2 k_n h}\left(h + \dfrac{\sinh 2k_n h}{2k_n}\right), & \text{for}\ \ n = 0 \\ \dfrac{1}{2\cos^2 k_n h}\left(h + \dfrac{\sin 2k_n h}{2k_n}\right), & \text{for}\ \ n = 1, 2, ... \end{cases}$$

$$V_n = \begin{cases} (h-d), & n = 0 \\ \dfrac{1}{2}(h-d), n = 1, 2, 3, ... \end{cases}$$

It may be noted that the gravity wave dispersion relations as in Equation (17) have one positive real root and infinitely many roots contribute to the velocity potentials as in Equations (14) and (16), where, the positive real root corresponds to the progressive wave mode and infinitely many roots corresponds to evanescent modes.

The unknown coefficients $A_{1mn}^{(S)}$, $A_{2mn}^{(S)}$, $A_{3mn}^{(S)}$ and $B_{2mn}^{(S)}$'s for $n = 0, 1, 2, ...$ and $m = 1, 2, ...$ associated with the radiation velocity potentials in Equations (14)–(16) are determined by using the condition of continuity of velocity and pressure at $x = \pm l$ along $0 \leqslant z \leqslant b$.

Continuity of velocity at the vertical interface $x = l$ as

$$\frac{\partial\varphi_{R1}^{(S)}}{\partial x} = \begin{cases} \delta_{2,S} + (y-y_0)\delta_{3,S} & \text{for}\ 0 < y < d, 0 \leqslant z \leqslant b \\ \dfrac{\partial\varphi_{R2}^{(S)}}{\partial x} & \text{for}\ d < y < h, 0 \leqslant z \leqslant b \end{cases} \tag{23a}$$

Continuity of velocity at the vertical interface $x = -l$ as

$$\frac{\partial\varphi_{R3}^{(S)}}{\partial x} = \begin{cases} \delta_{2,S} + (y-y_0)\delta_{3,S} & \text{for}\ 0 < y < d, 0 \leqslant z \leqslant b \\ \dfrac{\partial\varphi_{R2}^{(S)}}{\partial x} & \text{for}\ d < y < h, 0 \leqslant z \leqslant b \end{cases} \tag{23b}$$

Further, the continuity of pressure at the vertical interfaces $x = \pm l$ is given by

$$\varphi_{R1}^{(S)} = \varphi_{R2}^{(S)}\ \text{at}\ x = l, \text{for}\ d < y < h, 0 \leqslant z \leqslant b \tag{24a}$$

$$\varphi_{R2}^{(S)} = \varphi_{R3}^{(S)} \text{ at } x = -l \text{ for } d < y < h, 0 \leqslant z \leqslant b \tag{24b}$$

Substituting the velocity potentials from Equations (14) and (15) into the continuity of velocity condition (23a), multiplying both sides by the eigenfunction $u_{mj}(y,z)$ and then integrating with their respective intervals and keeping in mind the orthogonal relation u_{mj} for $j = 0, 1, 2, ...$, $m = 1, 2, ...$ in Equation (23), yields

$$\begin{aligned} &-\frac{b}{2} p_{m0} A_{1m0}^{(S)} U_0 - \frac{b}{2} \sum_{n=0}^{N} \alpha_{mn} \left(-A_{2mn}^{(S)} + B_{2mn}^{(S)} \mathrm{e}^{2\alpha_{mn} l} \right) \int_d^h u_0(y) v_n(y) \mathrm{d}y \\ &= \frac{b}{2} \int_0^{\mathrm{d}} \left[\{ \delta_{2,S} + (y - y_0) \delta_{3,S} \} + \delta_{3,S} \frac{\cosh \alpha_{m0}(h-y)}{\alpha_{m0} \sinh \alpha_{m0}(h-d)} \right] u_0(y) \mathrm{d}y \text{ for } n = 0 \end{aligned} \tag{25a}$$

$$\begin{aligned} &-\frac{b}{2} p_{mn} A_{1mn}^{(S)} U_n - \frac{b}{2} \sum_{n=0}^{N} \alpha_{mn} \left(-A_{2mn}^{(S)} + B_{2mn}^{(S)} \mathrm{e}^{2\alpha_{mn} l} \right) \int_d^h u_n(y) v_n(y) \mathrm{d}y \\ &= \frac{b}{2} \int_0^{\mathrm{d}} \left[\{ \delta_{2,S} + (y - y_0) \delta_{3,S} \} + \delta_{3,S} \frac{\cosh \alpha_{m0}(h-y)}{\alpha_{m0} \sinh \alpha_{m0}(h-d)} \right] u_n(y) \mathrm{d}y \text{ for } n = 1, 2, ..., N \end{aligned} \tag{25b}$$

where, the infinite series is truncated after N-terms and as the variable is a dummy j is replaced by n. Proceeding as in Equations (25a) and (25b) and using Equations (15)–(16) into the velocity continuity condition (23b), and applying the orthogonal relation (21), result in

$$\begin{aligned} &-\frac{b}{2} \mathrm{i} p_{m0} A_{3m0}^{(S)} W_0 - \frac{b}{2} \sum_{n=0}^{N} \alpha_{mn} \left(-A_{2mn}^{(S)} \mathrm{e}^{2\alpha_{mn} l} + B_{2mn}^{(S)} \right) \int_0^h u_0(y) v_n(y) \mathrm{d}y \\ &= \frac{b}{2} \left[\int_0^d \{ \delta_{2,S} + (y - y_0) \delta_{3,S} \} + \frac{\delta_{3,S}}{\alpha_{m0} \sinh \alpha_{m0}(h-d)} \int_d^h \cosh \left[\alpha_{m0}(h-y) \right] \right] u_0(y,z) \mathrm{d}y \text{ for } n = 0 \end{aligned} \tag{26a}$$

$$\begin{aligned} &\frac{b}{2} p_{mn} A_{3mn}^{(S)} U_n - \frac{b}{2} \sum_{n=0}^{N} \alpha_{mn} \left(-A_{2mn}^{(S)} \mathrm{e}^{2\alpha_{mn} l} + B_{2mn}^{(S)} \right) \int_0^h u_n(y) v_n(y) \mathrm{d}y \\ &= \frac{b}{2} \left[\int_0^d \{ \delta_{2,S} + (y - y_0) \delta_{3,S} \} + \frac{\delta_{3,S}}{\alpha_{m0} \sinh \alpha_{m0}(h-d)} \int_d^h \cosh \left[\alpha_{m0}(h-y) \right] \right] u_n(y) \mathrm{d}y \quad n = 1, 2, ..., N \end{aligned} \tag{26b}$$

Further, substituting Equations (14)–(15) into the pressure continuity condition (24a), and applying the orthogonal relation (22), obtained as

$$\begin{aligned} &\frac{b}{2} \sum_{n=0}^{N} A_{1mn}^{(S)} \int_0^b \int_d^h u_n(y) v_j(y) \mathrm{d}y - \frac{b}{2} \left(A_{2mj}^{(S)} + B_{2mj}^{(S)} \mathrm{e}^{2\alpha_{mj} l} \right) V_j \\ &= \frac{b}{2} \{ \delta_{1,S} - (l - x_0) \delta_{3,S} \} \int_d^h \frac{-\cosh \alpha_{m0}(h-y)}{\alpha_{m0} \sinh \alpha_{m0}(h-d)} v_j(y) \mathrm{d}y \\ &\text{for } j = 0, 1, 2, ..., N \end{aligned} \tag{27}$$

Similarly, by substituting Equations (15)–(16) into the pressure continuity condition (24b), and using the orthogonal relation (21), one can be obtained as

$$\begin{aligned} &\frac{b}{2} \sum_{n=0}^{N} A_{3mn}^{(S)} \int_d^h u_n(y) v_j(y) \mathrm{d}y - \frac{b}{2} \left(A_{2mj}^{(S)} \mathrm{e}^{2\alpha_{mj} l} + B_{2mj}^{(S)} \right) V_j \\ &= \frac{b}{2} \{ \delta_{1,S} + (l + x_0) \delta_{3,S} \} \int_d^h \frac{-\cosh \alpha_{m0}(h-y)}{\alpha_{m0} \sinh \alpha_{m0}(h-d)} v_j(y) \mathrm{d}y \\ &\text{for } j = 0, 1, 2, ..., N \end{aligned} \tag{28}$$

To solve the system of linear equations through numerical methods, the infinite series sums are truncated after the finite number of N-terms present in Equations (26)–(28). Thus, a linear system of equations $4(N+1)$ is obtained to solve for $4(N+1)$ number of unknown coefficients $A_{1mn}^{(S)}$'s, $A_{2mn}^{(S)}$'s, $A_{3mn}^{(S)}$'s and $B_{2mn}^{(S)}$'s for motion mode S that are associated with the eigenvalues k_n and β_n present in the expressions (14)–(16). Once the unknown coefficients are determined, then the full solution will be obtained in terms of radiation potentials.

3.2 Analytical expressions for wave forces and hydrodynamic coefficients

The wave forces in the frequency domain can be obtained by use of the known incident and the radiation potentials via the application of the Haskind theorem. The radiation force due to the heave, sway, and roll motions of the floating rectangular structure can be calculated from the radiation potentials in which the hydrodynamic coefficients such as added mass and damping coefficients

are involved.

The wave forces in terms of incident and radiation potentials can be expressed as

$$F_{ej} = \mathrm{i}\rho\omega\left[\int_{S_b}\phi_I(x,y,z)n_j\mathrm{d}s\mathrm{d}z - \int_{S_b}\phi_R^j(x,y,z)\frac{\partial\phi_I}{\partial n}\mathrm{d}s\mathrm{d}z\right] \tag{29}$$

where j=1, 2, S_b denotes the wetted surface in xyz-plane and n_j is the inward normal to the floating structure. Now, substituting Equations (3), (14), and (16) into Equation (29), which yields

$$F_{ej} = \left(F_I^j + F_D^j\right) \tag{30}$$

where F_I^j and F_D^j denote the forces due to the incident wave and because of the diffracted wave, respectively, with F_{e1}, F_{e2} and F_{e3} are refer to the vertical, horizontal, and torque acting on the floating structure. F_I and F_D denote the forces due to the incident wave and caused by the diffracted wave, respectively, and these expressions are

$$F_I = \frac{-\rho g I_{m0}\cosh\left[k_0(h-d)\right]}{\cosh(k_0h)}\frac{2\sin(lp)}{p} \tag{31a}$$

$$F_D = C_1\left\{C_P + \sum_{n=0}^{N}\left[A_{2n}C_{G1}(n) + B_{2n}C_{G2}(n)\right]\right\} + C_2\left\{\left(A_{30}\mathrm{e}^{\mathrm{i}lp} - A_{10}\mathrm{e}^{-\mathrm{i}lp}\right)I_1(0) + \sum_{n=1}^{N}\left(A_{3n}\mathrm{e}^{\mathrm{i}lp} - A_{1n}\mathrm{e}^{-\mathrm{i}lp}\right)I_1(n)\right\} \tag{31b}$$

where

$$C_P = \frac{2\sin(lp)}{p}C_F(d),\ C_F(d) = -\frac{\coth\left[\alpha_0(h-d)\right]}{\alpha_0},$$

$$C_1 = \frac{-\rho g k_0 I_{m0}\sinh\left[k_0(h-d)\right]}{\cosh(k_0h)},\ C_2 = \frac{-\mathrm{i}\rho g p I_{m0}}{\cosh(k_0h)},$$

$$C_{G1}(n) = \left(\frac{\mathrm{e}^{2\alpha_n l + \mathrm{i}lp} - e^{-\mathrm{i}lp}}{\mathrm{i}p + \alpha_n}\right)\cos\beta_n(h-d),$$

$$C_{G2}(n) = \left(\frac{\mathrm{e}^{\mathrm{i}lp} - \mathrm{e}^{2\alpha_n l - \mathrm{i}lp}}{\mathrm{i}p - \alpha_n}\right)\cos\beta_n(h-d),$$

$$I_1(0) = \frac{1}{\cosh(k_0h)}\int_0^d\cosh^2\left[k_0(h-y)\right]\mathrm{d}y,$$

$$I_1(n) = \frac{1}{\cos(k_nh)}\int_0^d\cos\left[k_n(h-y)\right]\cosh\left[k_0(h-y)\right]\mathrm{d}y.$$

3.3 Hydrodynamic coefficients such as added mass and radiation damping coefficients

Here, the radiation force is the force due to the motion of the floating structure which can be calculated from the radiation potentials. Now, the expression for the radiation force acting on and along the width of the structure is

$$\begin{aligned}F_R^j &= \int_{S_b}\mathrm{i}\rho\omega\phi_R^{(S)}\mathrm{e}^{-\mathrm{i}\omega t}n_j\mathrm{d}s\\ &= \rho\omega^2 I_R^{(S)}\mathrm{e}^{-\mathrm{i}\omega t}\int_{S_b}\phi_R^{(S)}n_j\mathrm{d}s\\ &= I_R^{(S)}\mathrm{e}^{-\mathrm{i}\omega t}\sum_{S=1}^{3}\left(\omega^2 M_{S,j}I_R^{(S)}\mathrm{e}^{-\mathrm{i}\omega t} + \mathrm{i}\omega I_R^{(S)}\mathrm{e}^{-\mathrm{i}\omega t}N_{S,j}\right)\end{aligned} \tag{32}$$

where $M_{S,j}$ and $N_{S,j}$ are the added mass and damping coefficients of the floating structure due to the motion mode S in jth direction, respectively and which expressions are given by

$$M_{S,j} = \mathrm{Re}\left(\rho f_{S,j}\right) \tag{33}$$

$$N_{S,j} = \mathrm{Im}\left(\rho\omega f_{S,j}\right) \tag{34}$$

with Re and Im denote to the real and imaginary parts of a complex expression, respectively with $f_{S,j}$ are given by

$$f_{S,1} = \int_0^b\int_{-1}^{l}\phi_{R2}^{(S)}\mathrm{d}x\mathrm{d}z \tag{35}$$

$$f_{S,2} = \int_0^b\int_0^d\left(-\phi_{R1}^{(S)}\Big|_{x=l} + \phi_{R3}^{(S)}\Big|_{x=-l}\right)\mathrm{d}y\mathrm{d}z \tag{36}$$

$$f_{S,3} = \int_0^b\left[\int_0^d\left(\phi_{R3}^{(S)}\Big|_{x=-l} - \phi_{R1}^{(S)}\Big|_{x=l}\right)(y-y_0)\mathrm{d}y + \int_{-l}^{l}\phi_{R2}^{(S)}\Big|_{y=d}(x-x_0)\mathrm{d}x\right]\mathrm{d}z \tag{37}$$

The non-dimensional added mass, damping coefficients, wave forces, and phase angle of wave forces of heave, sway, and roll motions are defined by

$$C_{aj} = \begin{cases}\dfrac{M_{j,j}}{(2\rho ld)} & \text{for } j = 1, 2\\ \dfrac{M_{j,j}}{(2\rho l^3 d)} & \text{for } j = 3\end{cases} \tag{38}$$

$$C_{dj} = \begin{cases} \dfrac{N_{j,j}}{(2\rho\omega l d)} & \text{for } j = 1, 2 \\ \dfrac{N_{j,j}}{(2\rho\omega l^3 d)} & \text{for } j = 3 \end{cases} \tag{39}$$

$$F_j = \begin{cases} \dfrac{|F_{ej}|}{(2\rho g l I_{m0})} & \text{for } j = 1, 2 \\ \dfrac{|F_{ej}|}{(2\rho g l I_{m0})} & \text{for } j = 3 \end{cases} \tag{40}$$

where I_{m0} is the same as in Equation (3). The next subsequent sections will check the computational accuracy of the solutions and several numerical results on hydrodynamic coefficients and wave forces of the heave, sway, and roll motions of the floating structure will be analyzed in different cases

4 Numerical model formulation and description

The description of the detailed numerical model principle is deferred here as it is the open-source BEM code NEMOH software (see for detail Babarit and Delhommeau, 2015).

The mathematical model adopted in this numerical implementation is similar to the one presented by Bispo et al. (2022a, b), bearing in mind that the numerical model presented here is designed as a rigid single module structure with no articulations. Based on the linear theory of waves, the total velocity potential with time-dependent can be written as $\Phi = \phi e^{-i\omega t}$, where ϕ is the total time-independent velocity potential, ω is the wave frequency rad/sec and t is the time. Then, one can describe the fluid with the velocity potential that can be decomposed into three parts ϕ_I, ϕ_D, and ϕ_R, respectively, based on the assumption of an ideal fluid and linearity and the velocity potential can be expressed as in Equation (2), satisfying the following boundary conditions:

$$\begin{cases} \nabla^2\phi = 0, & \text{in } \Omega \\ -\omega^2\phi + g\dfrac{\partial\phi}{\partial z} = 0, & \text{on } S_f \\ \dfrac{\partial\phi}{\partial n} = \boldsymbol{V}_{S_b}\cdot\boldsymbol{n}, & \text{on } S_b \\ \dfrac{\partial\phi}{\partial z} = 0, & \text{on } S_B \\ \lim\limits_{r\to\infty}\sqrt{r}\left[\dfrac{\partial\phi}{\partial r} - \dfrac{i\omega^2}{g}\phi\right] = 0, & \text{on } S_\infty \end{cases} \tag{41}$$

where g is the gravitational constant and r is the radial distance from the origin.

In this numerical BVP, the fluid domain is represented by Ω, S_f is the free surface, S_B is the bottom surface, S_∞ represents the boundary at infinity, and the wetted surface of the body is given by S_b, $\boldsymbol{n}$ is the unit vector normal to the wetted surface, pointing outwards, and $\boldsymbol{V}_{S_b}$ is the fluid velocity on the wet surface of the floating structure, as can be seen in Figure 2.

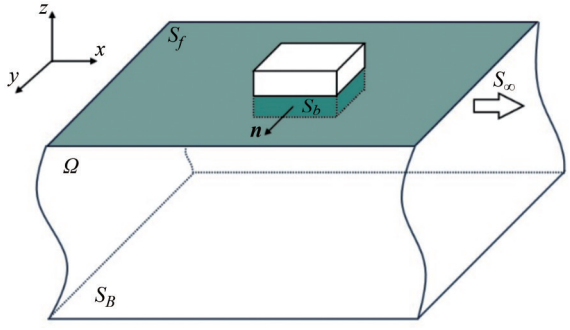

Figure 2 Schematic diagram of the floating body and the computational domain

Once the velocity potential, ϕ, is obtained, the added mass and the radiation damping can be computed. On the other hand, the excitation forces, F_{W_j}, can be related to the incident and diffraction potentials for the jth degree of freedom by:

$$F_{w_j} = \rho i\omega \iint_{\overline{S_b}} (\phi_I + \phi_D)\cdot\boldsymbol{n}\,dS_b \tag{42}$$

in which ρ is the fluid density, ω is the wave frequency, $\overline{S_b}$ is the mean wet surface of the body, and i is the complex unit.

The generalized added mass and radiation damping are given by:

$$\boldsymbol{a} + \frac{i}{\omega}\boldsymbol{b} = \rho \iint_{\overline{S_b}} \phi_R\cdot\boldsymbol{n}\,dS_b \tag{43}$$

where $\boldsymbol{a} = A_{jk}$ and $\boldsymbol{b} = B_{jk}$ are the added mass and radiation-damping coefficients of the jth mode induced by kth mode. For six degrees of freedom, the equation of motion of the free-floating body is presented in the frequency domain, and for unitary wave amplitude as (see Newman, 1977)

$$(\boldsymbol{M} + \boldsymbol{A}(\omega))\ddot{\boldsymbol{X}} + \boldsymbol{B}(\omega)\dot{\boldsymbol{X}} + \boldsymbol{K}\boldsymbol{X} = \boldsymbol{F}_W(\omega) \tag{44}$$

where $\boldsymbol{M}$ is a matrix of mass and inertias, matrix $\boldsymbol{K}$ is the hydrostatic stiffness matrix and it is defined similarly to the mass matrix, for 6 DOF. The added mass and radiation damping matrices, respectively represented by $\boldsymbol{A}(\omega)$ and $\boldsymbol{B}(\omega)$, are matrices of 6×6 size. The vector $\boldsymbol{X}$ represents the displacement, from which follows that $\dot{\boldsymbol{X}}$ and $\ddot{\boldsymbol{X}}$ are its first- and second-time derivatives, respectively. Lastly, $\boldsymbol{F}_W(\omega)$ is the vector of wave excitation forces.

5 Results and discussions

To make sure the correctness of the present analytical solution, the analytical results of wave forces are compared with numerical BEM code NEMOH simulations. Hereafter, all computations are executed throughout the paper by considering gravitational constant g=9.8 m/s^2 and water density ρ=1 025 kg/m^3 unless mentioned otherwise.

5.1 Comparison of analytical and numerical BEM code NEMOH simulations

Figures 3(a)–(c) show the comparison of present and numerical BEM code NEMOH of vertical wave force (heave motion) result with m=1, and versus non-dimensional wavenumber k_0h. It is seen that the results of the vertical wave forces from the analytical solution are a similar trend and have a good agreement with the results from numerical BEM code NEMOH.

On the other hand, Figure 3(d) compares the result of vertical wave force acting on the floating structure between present (analytical) and experimental data available in Rodriguez and Spinneken (2016) versus non-dimensional wavenumber k_0b. It is observed that the non-dimensional vertical force is well agreed for intermediate values of k_0b and the trend is similar between the present analytical and existing published experimental data. To quantify the comparison, the analytical result in Figure 3(d) represents 90% of the predicted value of the vertical force and this simple approximation can be considered a good fit for $0.5 \leqslant k_0b \leqslant 0.9$, whereas the discrepancy is less than 10% in the ranges $k_0b<0.4$ and $k_0b>1.0$.

5.2 Wave forces, hydrodynamic coefficients, and their comparison analysis for different design parameters

To understand the effect of design parameters associated with the BVP, this subsection will present several numerical results on the vertical wave force, horizontal wave force, and torque on the floating rectangular box-type structure by analyzing the effect of mode of oscillation, non-dimensional length, width, and draft due to the heave, sway, and roll motions in different cases.

Figure 4 represents the effect of modes of oscillation m on the non-dimensional vertical wave force F_1, horizontal wave force F_2, torque F_3, comparison between F_1, F_2, and F_3 of heave, sway, and roll motions with b/h=0.6, l/h = 0.5 and d/h=0.6 versus non-dimensional wavenumber k_0h. It is observed that the non-dimensional horizontal force, vertical wave force, and torques increase with an increase in modes of oscillation m. This is attributed to the fact that a group of small amplitude waves is generated at the edges of the floating box which reach a certain amount of incident wave en-

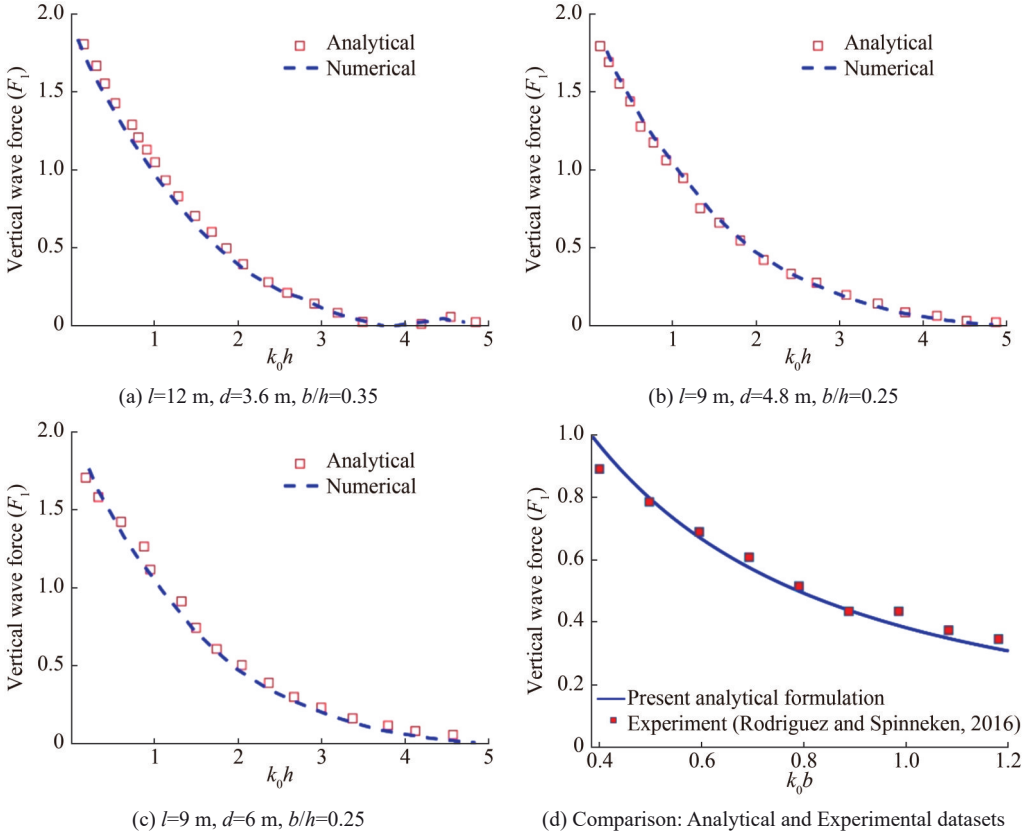

(a) l=12 m, d=3.6 m, b/h=0.35

(b) l=9 m, d=4.8 m, b/h=0.25

(c) l=9 m, d=6 m, b/h=0.25

(d) Comparison: Analytical and Experimental datasets

Figure 3 Comparisons of vertical wave force F_1 among analytical, numerical BEM code NEMOH and experimental datasets

ergy that makes higher loads on the box. Further, it is also found that the vertical force values are the least among the horizontal wave force and torque that is $F_1 < F_3 < F_2$. In addition, in Figure 4(d), the vertical wave force is 0.3 m, while the torque is 0.1 m which is 20% larger.

In Figure 5, the effects of non-dimensional structural length l/h on the non-dimensional vertical wave force F_1, horizontal wave force F_2, torque F_3, and comparison of F_1, F_2, F_3 for $d/h = 0.5$, $b/h = 0.8$, and $m = 1$ versus k_0h are plotted. It is observed that the vertical and horizontal wave forces become higher for longer structures whilst, this effect is the opposite trend in the case of torque to that of vertical and horizontal wave forces. In Figure 5(d), the comparison of wave forces indicated that the horizontal wave force is 4.2 m, while the vertical load is 3.6 m which is 60% larger. Further, in Figures 5(b)−(d), it is seen that the wave forces attained minimum values for a certain wavenumber k_0h, which is due to phase change of incident and reflected waves leading to constructive/destructive interference of the waves at the edges of the floating box.

Figure 6 plots the effect of non-dimensional structural width b/h on the non-dimensional vertical wave force F_1, horizontal wave force F_2, torque F_3, and their comparison with $m = 1$, $d/h = 0.5$ and $l/h = 0.8$ versus k_0h. In general, it is observed that for larger structural widths, the vertical and horizontal wave forces and torques decrease with occurring significant effect for smaller values k_0h. Also, the vertical wave force values are the least among the horizontal wave force and torque that is $F_1 < F_3 < F_2$. From Figures 5−6, it is concluded that the size of the floating box is important, especially when considering the wave forces as the horizontal force to the vertical force may change significantly depending on the length and width of the structure.

In Figure 7, the effects of the draft d/h on the non-dimensional vertical wave force F_1, horizontal wave force F_2, torque F_3, and comparison of F_1, F_2, and F_3 with $m = 1$, $l/h = 0.8$, and $b/h = 0.8$ versus k_0h are plotted. It is observed that the vertical wave forces become higher with a smaller draft whilst, the horizontal force increases with an increase in the values of d/h. However, the pattern of vertical force is opposite in trend to that of horizontal force. This is due to the deeper drafts leads smaller force in vertical and more horizontal wave force on the floating box. Further, the observations in Figure 7(d) are similar to Figure 6(d).

Figure 8 presents the effect of non-dimensional width b/h on the non-dimensional added mass C_{aj} for the heave, sway, and roll motions of the structure with $m = 1$, $d/h = 0.5$ and $l/h = 0.8$ versus k_0h. From Figures 8(a)−(c), it is seen that the added mass of heave, sway, and roll becomes higher for wider structure whilst, in the case of sway motion, the variations for different values of width become negligible for higher values of non-dimensional wavenumber.

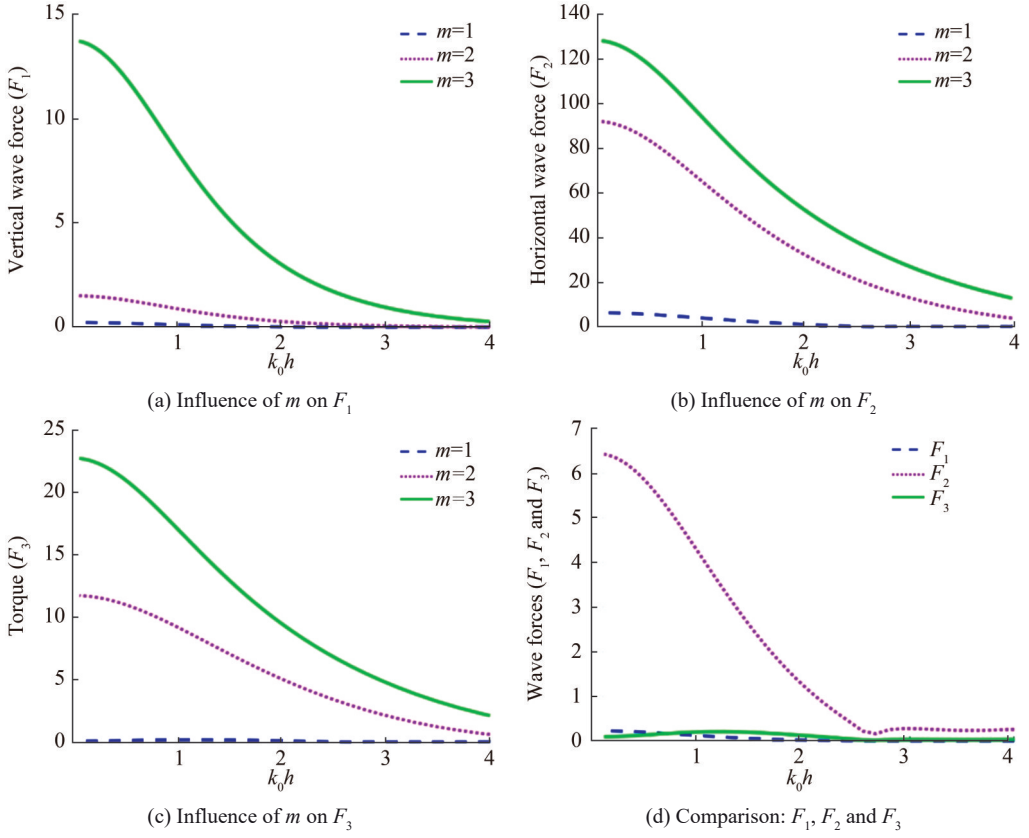

(a) Influence of m on F_1

(b) Influence of m on F_2

(c) Influence of m on F_3

(d) Comparison: F_1, F_2 and F_3

Figure 4 Effect of modes of oscillation on the non-dimensional wave forces F_1, F_2, F_3 versus k_0h and comparison among them

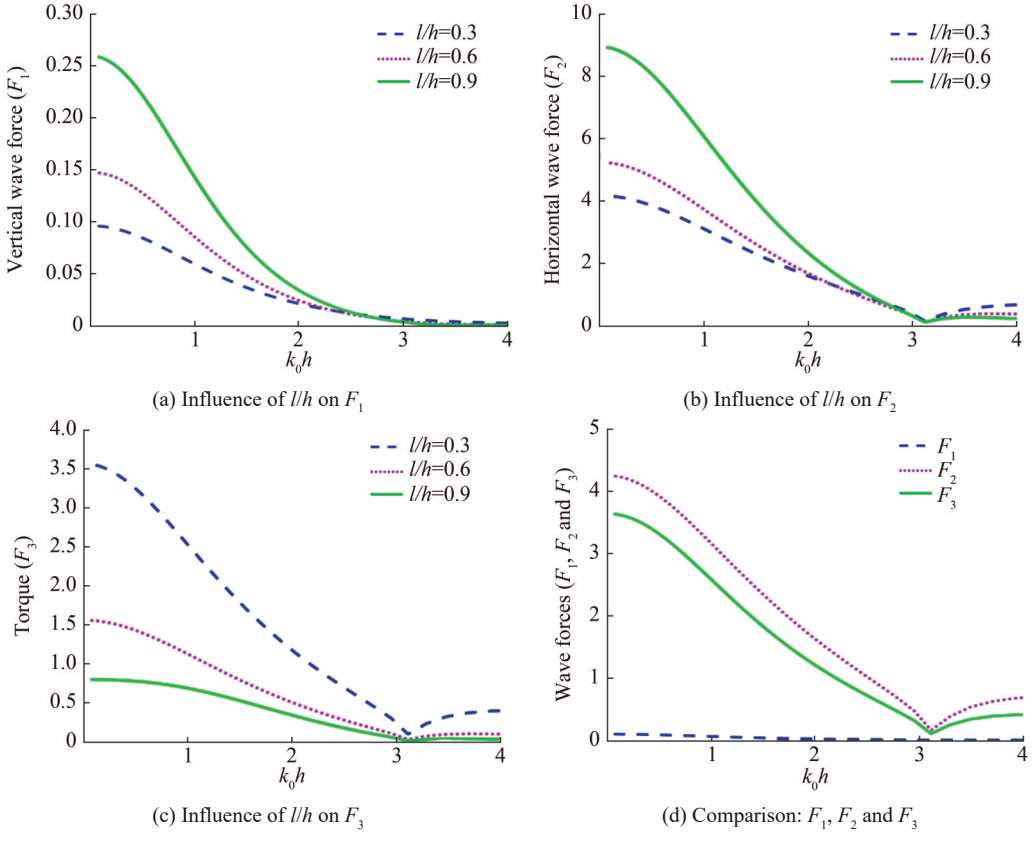

(a) Influence of l/h on F_1

(b) Influence of l/h on F_2

(c) Influence of l/h on F_3

(d) Comparison: F_1, F_2 and F_3

Figure 5 Effect of structural length on F_1, F_2, F_3, and comparison among them for m=1

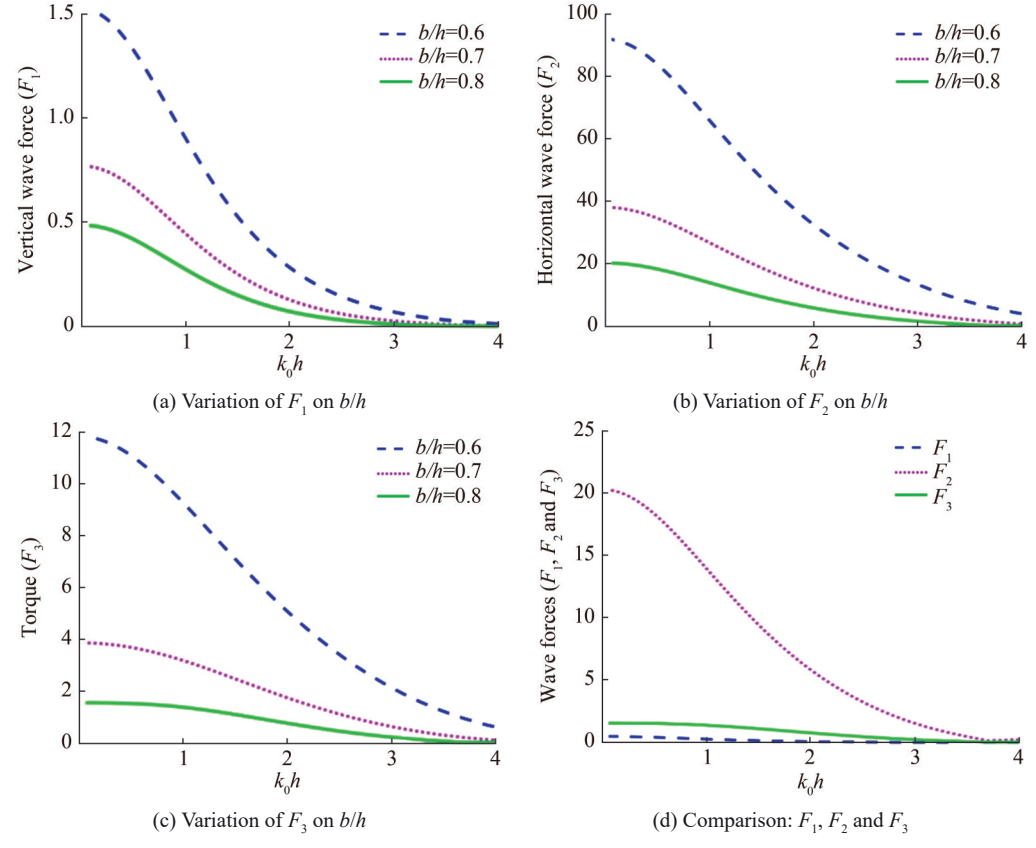

(a) Variation of F_1 on b/h

(b) Variation of F_2 on b/h

(c) Variation of F_3 on b/h

(d) Comparison: F_1, F_2 and F_3

Figure 6 Effect of the structural width on the F_1, F_2, F_3, and their comparison for m=1

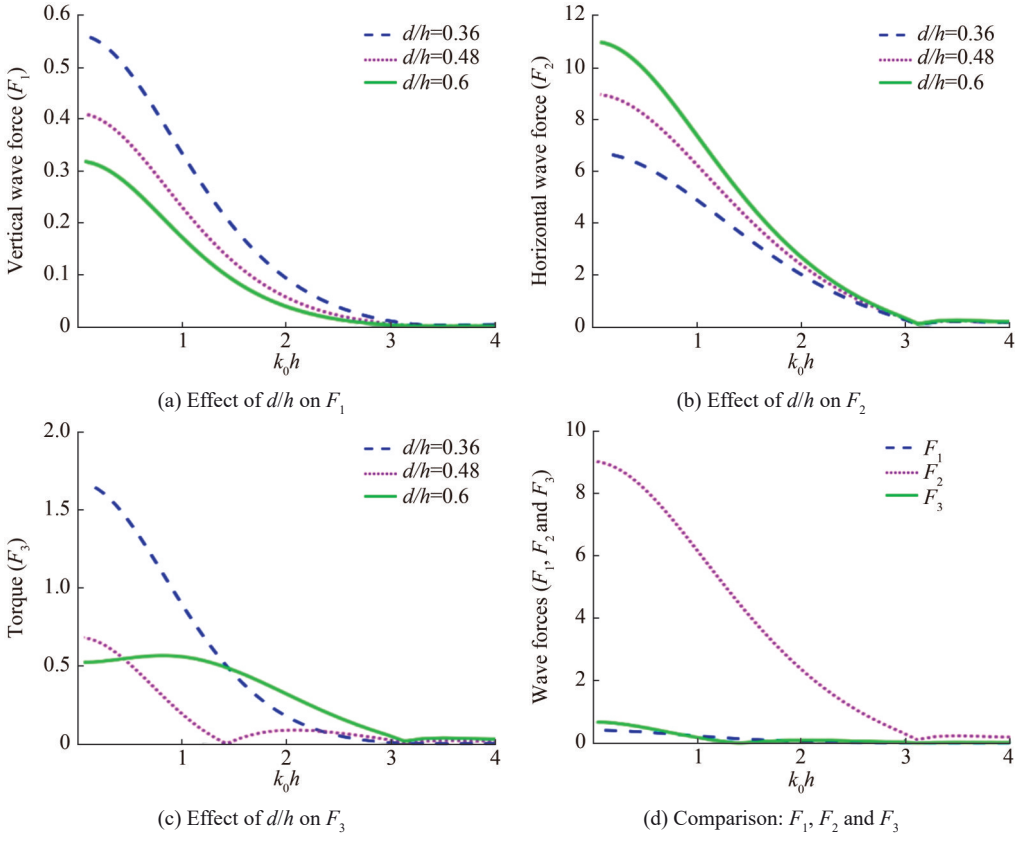

(a) Effect of d/h on F_1 (b) Effect of d/h on F_2

(c) Effect of d/h on F_3 (d) Comparison: F_1, F_2 and F_3

Figure 7 Effect of the structural drafts on the F_1, F_2, F_3, and comparison among them with $m = 1$

This is because the mass of the structure increases which leads to the more added mass.

Figure 9 depicts the effect of non-dimensional width b/h on the non-dimensional damping coefficients C_{dj} for the heave, sway, and roll motions of the structure with $m = 1$, $d/h = 0.5$ and $l/h = 0.8$ versus k_0h. It is observed that the damping coefficients of heave, sway, and roll decrease with an increase in non-dimensional structural width b/h whilst, the damping coefficients of roll increase with an increase in structural width $k_0h \leqslant 2.5$. This is attributed to the fact that as the structural width is increased while the draft and mode of oscillation (primary mode m=1) are kept fixed as a result the mass of the structure increases too which leads to less damping. The observations of the damping coefficients heave and sway is similar to those of Zheng et al. (2006).

5.3 Effect of design parameters on the reflection and transmission coefficients

Figure 10 plots the effect of non-dimensional width b/h on the reflection and transmission coefficients for $m = 1$, $l/h = 0.8$ and $d/h = 0.5$ versus k_0h. It is observed that the influences of the width on the reflection and transmission coefficients are appreciable. The maximum reflection coefficient and the minimum transmission coefficients greatly increase and decrease respectively with increases in the values of structural width.

In Figure 11, the influences of the d/h on the reflection coefficient K_r and the transmission coefficient K_t with $m = 1$, $l/h = 0.8$, and $b/h = 0.5$ versus k_0h are plotted. From Figure 11, it is seen that the effects of the width on the reflection and transmission coefficients are significant. The maximum reflection coefficient and the minimum transmission coefficients greatly increase and decrease, respectively with increases in the values of the structural draft. This is because less wave energy passes below the floating box as it expected wave reflection becomes more in the upstream region.

In Figure 12, the effects of the structural length l/h on the reflection coefficient K_r and transmission coefficient K_t with $m = 1$, $l/h = 0.8$, and $b/h = 0.5$ versus k_0h are plotted. For a smaller value of k_0h, the variations and effects of the structural length on the K_r and K_t are significant whilst, for $k_0h \geqslant 5$, the values of the K_r becomes zero and K_t attends one which leads physically true. Further, $k_0h \leqslant 5$, the reflection coefficients increase whilst, the pattern of the transmission coefficients becomes reveres to that of K_r. This is because the structure with a longer length has a larger projected area, which results in a larger hydrodynamic force that leads to higher reflection and lower transmission.

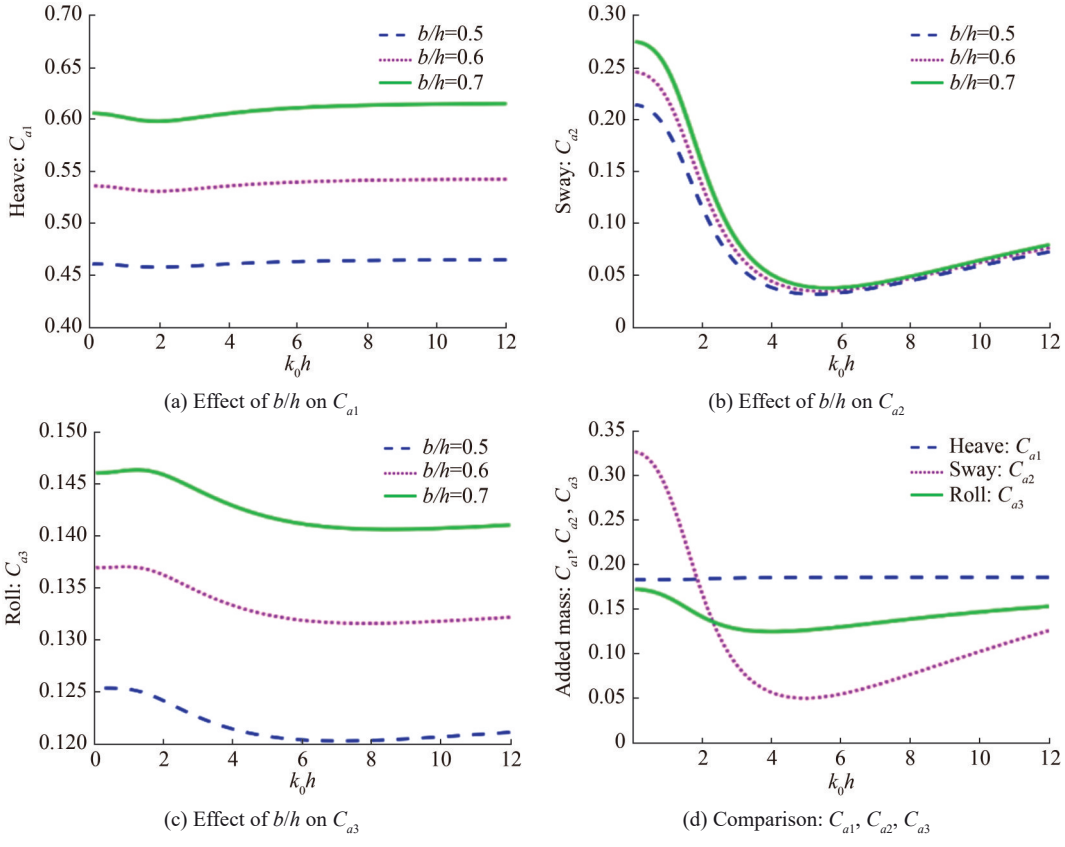

(a) Effect of b/h on C_{a1}

(b) Effect of b/h on C_{a2}

(c) Effect of b/h on C_{a3}

(d) Comparison: C_{a1}, C_{a2}, C_{a3}

Figure 8 Effect of width on the added masses C_{aj} and comparison among them with m = 1, l/h = 0.8 and d/h = 0.5

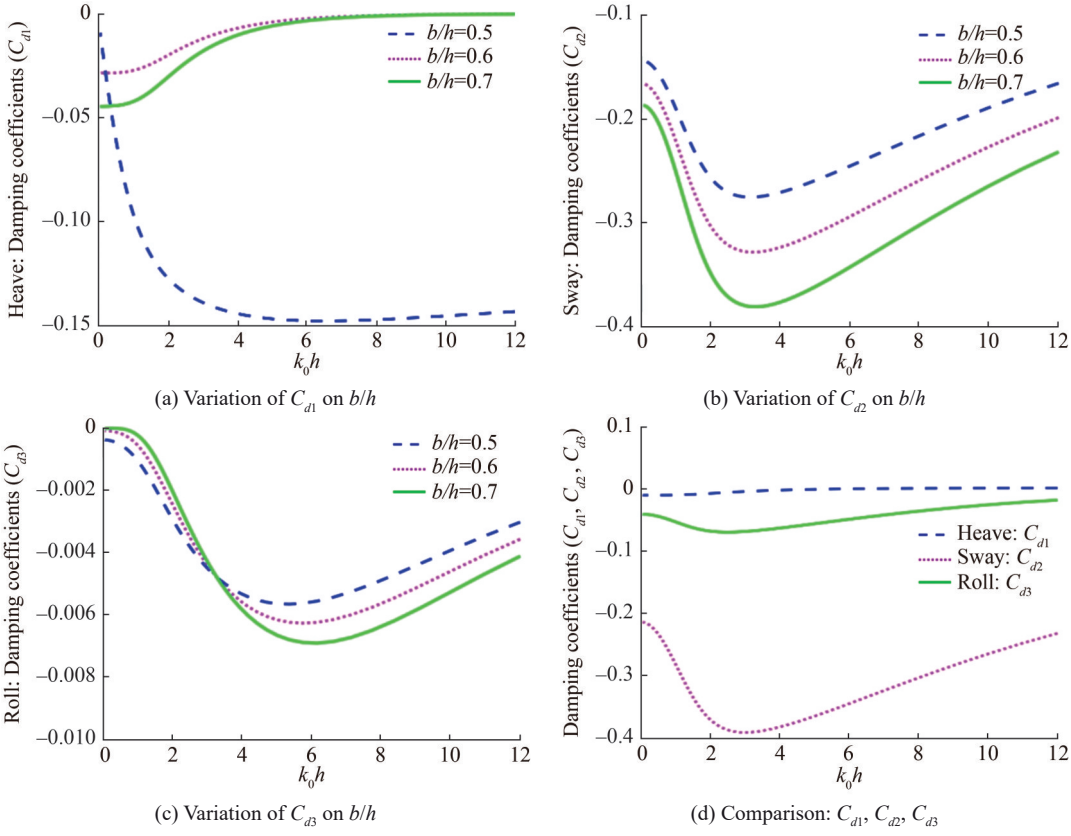

(a) Variation of C_{d1} on b/h

(b) Variation of C_{d2} on b/h

(c) Variation of C_{d3} on b/h

(d) Comparison: C_{d1}, C_{d2}, C_{d3}

Figure 9 Effect of width on the damping coefficients C_{dj} and comparison among them for m = 1, l/h = 0.8 and d/h = 0.5

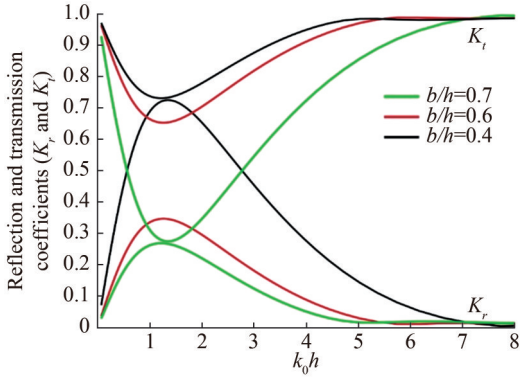

Figure 10 Effect of structural width on the reflection and transmission coefficients for $m = 1$, $l/h = 0.8$ and $d/h = 0.5$

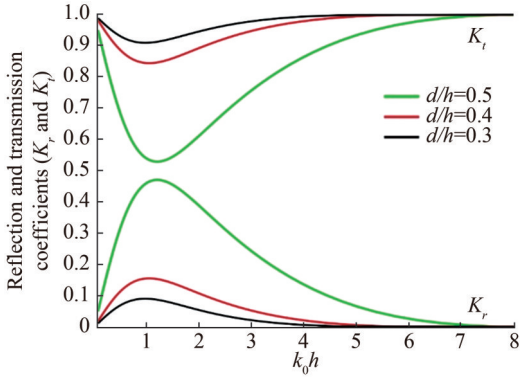

Figure 11 Effect of the structural draft on the reflection and transmission coefficients for $m = 1$, $l/h = 0.8$ and $b/h = 0.5$

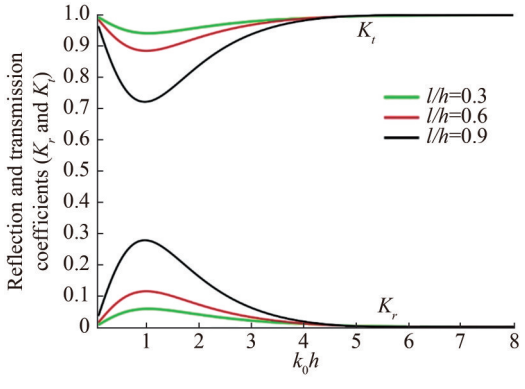

Figure 12 Effect of l/h on the K_r and K_t for $m = 1$, $l/h = 0.8$ and $b/h = 0.5$

6 Conclusions

The new contributions to the present compared with the previous research by Guo et al. (2018) (associated with diffraction) and Islam et al. (2019) (related with radiation) in oblique waves are the mathematical formulation on wave radiation by 3D floating box, analytical expressions for radiation potentials in three-dimensions and comparison with numerical BEM code based NEMOH simulations. Further, the results of wave forces and hydrodynamic coefficients such as added mass, damping coefficients, and wave quantities (reflection and transmission coefficients) for different design parameters are analyzed. From the present analysis, the following important conclusions are drawn.

1) In the verification of the analytical results, it is observed that the analytical results of vertical wave forces for different design parameters are well agreed with the numerical NEMOH and supported by the existing published experimental data sets.

2) It is observed that the vertical and horizontal forces and torques become higher for higher modes of oscillation m which because of the group of small amplitude waves generated at the edges of the floating box.

3) The comparisons for the different structural widths, lengths, drafts, and modes of oscillations on the wave forces for the heave, sway, and roll motions revealed that the wave forces among them hold the relation $F_1 < F_3 < F_2$.

4) The comparison between the non-dimensional added masses of heave, sway, and roll motions indicated that $C_{a2} < C_{a3} < C_{a1}$, whilst the damping coefficients hold the relationship $C_{d2} < C_{d3} < C_{d1}$ irrespective of k_0h.

5) It is observed that the reflection coefficients become higher for wider structures and this effect attends lower when the draft of the structure increases, whilst the trend of the transmission coefficient becomes reveres to that of reflection coefficients.

6) The above analysis indicated that the size of the floating box is important when considering the wave forces as the horizontal force to the vertical force may change significantly depending on the modes of oscillations, structural length, and width.

7) The present analysis will be helpful to model a large floating breakwater by articulating several floating box modules over analytical and numerical approaches to analyze the performance for the floating breakwater.

Funding This paper contributes to the project Hydroelastic behaviour of horizontal flexible floating structures for applications to Floating Breakwaters and Wave Energy Converters (HYDROELASTWEB), which is co-funded by the European Regional Development Fund (Fundo Europeu de Desenvolvimento Regional-FEDER) and by the Portuguese Foundation for Science and Technology (Fundação para a Ciência e a Tecnologia-FCT) under contract 031488_770 (PTDC/ECI-EGC/31488/2017). The first author was contracted as a Researcher by FCT, through Scientific Employment Stimulus, Individual support under Contract No. CEECIND/04879/2017. This work also contributes to the Strategic Research Plan of the Centre for Marine Technology and Ocean Engineering (CENTEC), which is financed by the Portuguese Foundation for Science and Technology (Fundação para a Ciência e Tecnologia-FCT) under contract UIDB/UIDP/00134/2020.

Competing interest C. Guedes Soares is one of Editors for the Journal of Marine Science and Application and was not involved in the editorial review, or the decision to publish this article. All authors declare that there are no other competing interests.

References

Babarit A, Delhommeau G (2015) Theoretical and numerical aspects of the open source BEM solver NEMOH. Proceedings of the 11th European Wave and Tidal Energy Conference (EWTEC2015), Nantes. https://hal.science/hal-01198800v1

Bispo IBS, Mohapatra SC, Guedes Soares C (2022a) Numerical analysis of a moored very large floating structure composed by a set of hinged plates. Ocean Engineering 253: 110785. https://doi.org/10.1016/j.oceaneng.2022.110785

Bispo IBS, Mohapatra SC, Guedes Soares C (2022b) Numerical model of a WEC-type attachment of a moored submerged horizontal set of articulated plates. In: Guedes Soares C, Santos TA (Eds.). Trends in Maritime Technology and Engineering, Taylor & Francis Group, London, Vol. 2, 335-344

Bhattacharjee J, Guedes Soares C (2011) Oblique wave interaction with a floating structure near a wall with stepped bottom. Ocean Engineering 38(13): 1528-1544. https://doi.org/10.1016/j.oceaneng.2011.07.011

Cho II-H (2016) Transmission coefficients of a floating rectangular breakwater with porous side plates. International Journal of Naval Architecture and Ocean Engineering 8(1): 53-65. https://doi.org/10.1016/j.ijnaoe.2015.10.002

Drimer N, Agnon Y, Stiassnia M (1992) A simplified analytical model for a floating breakwater in water of finite depth. Applied Ocean Research 14(1): 33-41. https://doi.org/10.1016/0141-1187(92)90005-5

Elchahal G, Younes R, Lafon P (2009) Parametrical and motion analysis of a moored rectangular floating breakwater. Journal of Offshore Mechanics and Arctic Engineering 131(3): 031303-1-11. https://doi.org/10.1115/1.3124125

Gadelho JFM, Mohapatra SC, Guedes Soares C (2018) CFD analysis of a fixed floating box-type structure under regular waves. In: Guedes Soares C, Ângelo P. Teixeira (Eds.). Developments in Maritime Transportation and Harvesting of Sea Resources, Taylor & Francis, London, 513-520

Guo Y, Mohapatra SC, Guedes Soares C (2018) Wave interaction with a rectangular long floating structure over flat bottom. In: Guedes Soares C, Santos TA (Eds.). Progress in Maritime Technology and Engineering, Taylor & Francis Group, London, 647-654

Islam H, Mohapatra SC, Guedes Soares C (2019) OpenFOAM analysis of the wave radiation by a box-type floating structure. Ocean Engineering 193: 106532. https://doi.org/10.1016/j.oceaneng.2019.106532

Lee JF (1995) On the heave radiation of the rectangular structure. Ocean Engineering 22(1): 19-34. https://doi.org/10.1016/0029-8018(93)E0009-H

McCartney BL (1985) Floating breakwater design. J Waterway Port Coast Ocean Engineering 111(2): 304-317. https://doi.org/10.1061/(ASCE)0733-950X(1985)111:2(304)

Mohapatra SC, Guedes Soares C (2019) Interaction of ocean waves with floating and submerged horizontal flexible structures in three-dimensions. Applied Ocean Research 83: 136-154. https://doi.org/10.1016/j.apor.2018.10.009

Mohapatra SC, Guedes Soares C (2022) 3D hydroelastic modelling of fluid-structure interactions of porous flexible structures. Journal of Fluids and Structures 112: 103588. https://doi.org/10.1016/j.jfluidstructs.2022.103588

Mohapatra SC, Guedes Soares C (2021) Hydroelastic behaviour of a submerged horizontal flexible porous structure in three-dimensions. Journal of Fluids and Structures 104: 103319. https://doi.org/10.1016/j.jfluidstructs.2021.103319

Newman JN (1977) Marine hydrodynamics. The M. I. T. Press, Cambridge, USA

Rodriguez M, Spinneken J (2016) A laboratory study on the loading and motion of a heaving box. Journal of Fluids and Structures 64: 107-126. https://doi.org/10.1016/j.jfluidstructs.2016.05.001

Zheng YH, You YG, Shen YM (2004) On the radiation and diffraction of water waves by a rectangular buoy. Ocean Engineering 31(8-9): 1063-1082. https://doi.org/10.1016/j.oceaneng.2003.10.012

Zheng YH, Shen YM, You YG, Wu BJ, Jie DS (2006) Wave radiation by a floating rectangular structure in oblique sea. Ocean Engineering 33(1): 59-81. https://doi.org/10.1016/j.oceaneng.2005.04.005